Inorganic Chemistry

Article

pubs.acs.org/IC

Experimental and Theoretical High-Energy-Resolution X-ray Absorption Spectroscopy: Implications for the Investigation of the Entatic State

Nora Jenny Vollmers,[†,§] Patrick Müller,[‡,§] Alexander Hoffmann,[⊥] Sonja Herres-Pawlis,[⊥] Martin Rohrmüller,[†] Wolf Gero Schmidt,[†] Uwe Gerstmann,*[,†] and Matthias Bauer*[,‡]

[‡]Department Chemie and [†]Department Physik, Universität Paderborn, Warburger Straße 100, D-33098 Paderborn, Germany

[⊥]Institut für Anorganische Chemie, RWTH Aachen University, Landoltweg 1, D-52074 Aachen, Germany

Supporting Information

ABSTRACT: High-energy-resolution-fluorescence-detected X-ray absorption near-edge structure (HERFD-XANES) spectroscopy is shown to be a sensitive tool to investigate the electronic changes of copper complexes induced by geometric distortions caused by the ligand backbone as a model for the entatic state. To fully exploit the information contained in the spectra gained by the high-energy-resolution technique, (time-dependent) density functional theory calculations based on plane-wave and localized orbital basis sets are performed, which in combination allow the complete spectral range from the prepeak to the first resonances above the edge step to be covered. Thus, spectral changes upon oxidation and geometry distortion in the copper *N*-(1,3-dimethylimidazolidin-2-ylidene)quinolin-8-amine (DMEGqu) complexes $[Cu^{I}(DMEGqu)_2](PF_6)$ and $[Cu^{II}(DMEGqu)_2](OTf)_2 \cdot MeCN$ can be accessed.

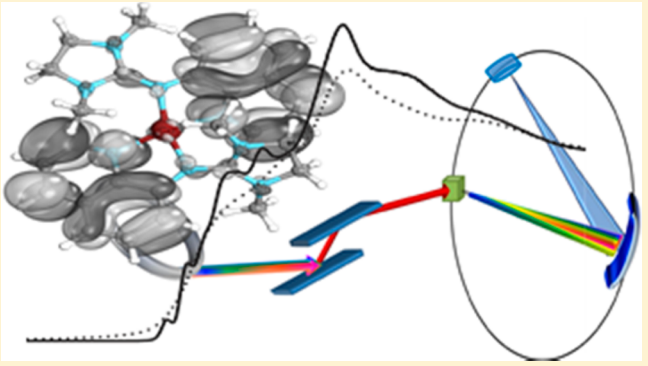

INTRODUCTION

Copper plays a central role in many electron-transfer (ET) processes in nature.[1] Blue copper, or type I, proteins span a large window of reduction potentials, which leads to a variety of possible ET partners.[1,2]

Although in nature copper is mostly bound to sulfur in such proteins, it was already reported that hard donor atoms also work in biomimetic ET systems with possibly advantageous properties regarding lifetimes of the catalytic site.[3] These nonblue systems exhibit ET features similar to those of type I proteins, but without sulfur donors and having a broader axial electron paramagnetic resonance hyperfine splitting, leading to the name "type-zero" compounds. The geometrical distortion between cuprous and cupric sites plays a central role for the efficiency of such ETs. Studying copper type-zero complexes with nitrogen-donor ligands using X-ray spectroscopic and theoretical techniques can therefore significantly contribute to the understanding of copper-mediated ET processes.

The ability to tune the Cu^{I}/Cu^{II} redox couple is crucial not only in nature but also for catalytic applications of biomimetic complexes. The reduction potential of the Cu^{I}/Cu^{II} redox pair is influenced by the electronic and structural parameters at the copper coordination site. In particular, the inner coordination sphere is dominating these parameters and has been subjected to many studies.[4−6] In the case of enzymes, those constraints are caused by the protein backbone, leading to a situation named rack-induced or entatic state, which facilitates ET from the kinetic point of view.[7,8]

In such states, deviations from the geometry obtained by ligand-field theory appear. Considering the Cu^{I}/Cu^{II} redox couple, the according geometries would be square-planar for Cu^{II} and tetrahedral for Cu^{I}. Changes in the redox state require therefore a change in the coordination symmetry. Any (even small) geometry deviation from the ligand-field limit facilitates the interconversion of the Cu^{I}/Cu^{II} redox states, enabling exceptionally fast ET. In the last years, many efforts have been invested in the synthesis of conformationally invariant copper(I/II) complexes as model complexes for the entatic state, but good models are still rare,[7,9−15] and the nature of the resulting entatic state is controversially discussed.[16−18] While some authors favor an electronic entatic state,[13] others claim geometric strain by the ligands to be the origin of the deviation from the theoretical ligand-field geometry.

It is thus a mandatory task to access experimentally the electronic (d-electron density) and geometric (arrangement of coordinating ligands) structures at the copper center to further understand the working principle of entatic model complexes. Single-crystal diffraction is surely the working horse for this purpose. However, it cannot be applied in the in situ

Received: July 20, 2016
Published: November 4, 2016

DOI: 10.1021/acs.inorgchem.6b01704
Inorg. Chem. 2016, 55, 11694−11706

environment of biomimetic compounds, i.e., in solution. Here, only short-range sensitive methods will give the desired information.

X-ray absorption spectroscopy (XAS) is the only element-specific method to achieve this aim. If hard-X-ray XAS at the copper K-edge is used, it has the advantage of delivering geometric and electronic structural parameters independent of the sample environment and can therefore be applied also under biorelevant in situ conditions.[19] Many successful applications of XAS on biomimetic copper complexes and related systems are known in the literature. They mainly focus on the structure information in the extended X-ray absorption fine structure (EXAFS) spectra.[20−22] These studies underline the spectroscopic prowess of XAS in this context. However, the full potential of the X-ray absorption near-edge structure (XANES) region, in which details about both the geometric (backscattering) and electronic (orbital contributions) situations are contained, could not be fully used. This is due to the lifetime broadening of the 1s electron−hole after K-edge excitation.[23,24] This broadening limits the extraction of information from the preedge peak and XANES region significantly.[25] Both spectral parts are broadened in such a way that details of the lowest unoccupied molecular orbital (LUMO) states above the Fermi level, which are highly sensitive to geometric changes, are masked and the characteristic first resonances after the edge are smeared out.[23]

The recent development of high-energy-resolution-fluorescence-detected XANES (HERFD-XANES) offers a powerful tool to overcome this limitation.[23] With this method, the lifetime broadening effect can be reduced significantly, and the fine structure in the prepeak and XANES spectra can be resolved. This allows a detailed comparison with theoretical calculations.

However, the computational XANES modeling faces a variety of challenges. On the one hand, the requirement to treat core−hole excitations renders the straightforward application of pseudopotential methods difficult. All-electron calculations, which appear particularly suitable for describing XAS, suffer from significantly larger computational costs than those required by pseudopotential-based methods. On the other hand, the description of excited states is, strictly speaking, beyond the realm of density functional theory (DFT), the method of choice for the description of complex structures. DFT neither accounts for the quasiparticle character of the electrons nor describes electron−hole attraction effects. There are well-founded and successful strategies[26] to overcome these limitations, e.g., the GW approximation for the electronic self-energies, where they are expressed as a convolution of the single-particle propagator G and the dynamically screened Coulomb interaction W, and the Bethe−Salpeter equation (BSE) approach to describe Coulomb-coupled electron−hole pairs.[27] However, these methodologies are prohibitively expensive for complex structures. In particular, far-edge regions cannot be easily computed within GW-BSE. Obviously, electron correlation methods such as coupled-cluster (CC) theory also give accurate access to excited states and thus can be used to determine X-ray excitations.[28−30] Again, the method is highly expensive, even if multilevel coupled-cluster (MLCC) implementations appear promising.[31]

Time-dependent DFT (TD-DFT) is numerically less demanding and thus presently the method of choice to address charge-neutral excitations in complex molecules. It is also frequently used to determine core excitations.[32−35] This approach is well-founded in principle, but the complication is hidden in the unknown time-dependent exchange and correlation (XC) potential that appears in the Kohn−Sham equations. Most numerical implementations rely on the adiabatic approximation, which often proves successful for finite systems such as molecules but fails for extended systems such as solids.[36] Constrained and orthogonality constrained density functional theories (cDFT[37] and OCDFT[38,39]) are possible alternative approaches to excited-state configurations.

A third difficulty in simulating XAS data is related to the basis set used to expand the electronic wave functions. Localized basis functions such as Gaussians are computationally efficient and do thus allow for the modeling of core electrons as well as many-body effects, e.g., by means of TD-DFT, even for comparatively complex structures; see., e.g., ref 40. However, they do not form a complete set and are not suitable for the description of excited high-energy states that typically are fairly delocalized. Plane waves, on the other hand, form by the construction of a complete and orthogonal basis set, the numerical convergence of which can be smoothly varied and reliably controlled. Moreover, plane waves are ideally suited to describe delocalized high-energy states as well as systems with periodic boundary conditions such as molecular crystals.[41] Naturally, the description of core states with plane waves is cumbersome.

In order to deal with these complications, we use two different and to some extent complementary theoretical approaches to simulate XANES: On the one hand, for molecular species, we use TD-DFT with a localized orbital basis set that is expected to be particularly suitable for the description of preedge peaks.[42] On the other hand, we used the continued-fraction expansion of Green's function[43−45] in conjunction with a plane-wave basis set, which appears particularly suited for solids, e.g., molecular crystal structures.[46] Here, the incorporation of the 1s core−hole into pseudopotentials[47,48] allows for a computationally very efficient cDFT-like description of excitonic effects involving core states[49] and also K-edge XAS spectra in a broad energy range. It has been used to describe the prepeak region of copper compounds[50] but results in a particularly reliable description of near- and far-edge features of the absorption spectrum.[47,51−55]

Consequently, the purpose of this work is 3-fold: (i) to establish HERFD-XANES as a new high-resolution method to investigate copper-based biomimetic systems, (ii) to elucidate the capability of TD-DFT and the continued-fraction approach to simulate and rationalize such spectra, and (iii) to show that a combined application of these schemes is able to unravel many details of the molecular geometries, which can be used to answer questions related to the entatic state principle in biomimetic systems. As a prototype example for such systems, we use a pair of copper(I) and copper(II) complexes formed by the quinoline-based ligand *N*-(1,3-dimethylimidazolidin-2-ylidene)quinolin-8-amine (DMEGqu), namely, $[Cu^{I}(DMEGqu)_2](PF_6)$ and $[Cu^{II}(DMEGqu)_2](OTf)_2\cdot MeCN$.[56] These complexes are characterized by the fact that the structures of their cationic units are structurally very similar.

EXPERIMENTAL SECTION

HERFD-XANES Measurements. HERFD-XANES experiments were performed at beamline ID26 at the European Synchrotron Radiation Facility (ESRF) in Grenoble, France. For measurements at the copper K-edge (8979 eV), a Si(311) double-crystal monochromator was used. The maximum beam current was 200 mA with a ring energy of 6 GeV. For K-edge measurements, the solid samples were prepared as wafers using degassed cellulose as a binder to avoid self-absorption effects. Spectra were recorded at 30 K in a closed-cycle helium cryostat. The copper(I) samples were additionally prepared under an inert atmosphere in a glovebox. The spectrometer was kept under a helium atmosphere to reduce the absorption of fluorescence radiation. No signs

DOI: 10.1021/acs.inorgchem.6b01704
Inorg. Chem. 2016, 55, 11694−11706

of radiation damage could be detected in any sample within the acquisition time, and measurements were carried out on multiple spots.

DFT Calculations. *ORCA.* Copper K-edge transitions were calculated using the TD-DFT approach implemented in *ORCA3.0.2*.[33,57−59] In these calculations, the core properties were described by triple-ζ basis sets CP(PPP)[60] for the copper atom and Ahlrich's all-electron TZVP for all other atoms.[61−63] Geometry optimizations of ionized single molecules were carried out using *ORCA3.0.3* employing Ahlrich's TZVP on all atoms with TPSSh.[64] This is frequently considered the functional of choice for copper-related systems and has in particular been proven useful for the description of the structural and vibrational properties of quinoline−guanidine copper complexes.[65−68] Furthermore, the Grimme dispersion correction with Becke−Johnson damping (D3BJ) has been utilized.[69,70] XANES spectra have been calculated for different molecular structures, i.e., for the self-consistently optimized gas-phase (*ORCA*) geometries, for single molecules, the geometry of which is obtained from the experimentally determined crystal structures (X-ray diffraction) and for molecular structures based on the calculated solid-state geometries (QUANTUM ESPRESSO). Thereby, several XC functionals were tested, i.e., the meta-generalized gradient approximation (GGA) functional TPSS and its hybrid version TPSSh,[64] the hybrid GGA functional B3LYP,[71−74] and the semilocal GGA functionals BP86[75,76] and PBE.[77] To speed up the hybrid calculations, the RIJCOSX[78,79] approximation implemented in *ORCA* was used. A special DFT grid of seven was set for copper. The tight convergence criterion was imposed on all calculations. For further analysis of the results, we used the program *MOAnalyzer*.[80] The calculated spectra have all been shifted to match the copper K-edge: a shift of 33−44 eV was required for hybrid functionals and 216−233 eV for semilocal functionals. In addition to the shift, all spectra have been normalized to the intensity of a characteristic peak [in case of copper(II), the prepeak]. The discrete single-energy transitions have been subjected to Gaussian broadening, with a full width at half-maximum linearly rising with increasing excitation energy.

QUANTUM ESPRESSO. Periodic boundary conditions and a plane-wave basis were employed for the realistic modeling of molecular crystals using the *QUANTUM ESPRESSO* (QE) package[46] implementation of DFT. The QE package has also been used for XAS simulations based on the continued-fraction approach.[47,48] Specifically, the *Xspectra* code[46] is used in conjunction with gauge-including projector-augmented-wave (GIPAW) pseudopotentials. Within this PAW-XAS approach, the incorporation of the 1s core−hole into the copper pseudopotentials allows for a reliable, but computationally very efficient description of excitonic effects[49] using Lanzcos recursion scheme to expand Green's function.[43−45] For structure optimization as well as for the simulation of XAS spectra, the complete crystal structures, including the counterions [two PF_6^- in the case of copper(I) species and eight OTf^- as well as one acetonitrile molecule for the copper(II) species], have been used. Notably, the calculated XAS spectra do not change considerably if we truncate the structures and consider only one molecule and its counterion(s) within periodic boundary conditions. This corresponds to bisecting and quartering of the actual crystal unit cell for the copper(I) and copper(II) systems. The insensitivity of the XAS simulations with respect to this structural simplification indicates that the weak intermolecular coupling between the molecules has only a minor influence on the XAS spectra. The XAS spectra are calculated using the same *k*-point sampling as that for the self-consistent total-energy calculations. A 2 × 2 × 2 *k*-point sampling and a cutoff energy of 90 Ry lead to numerically converged results for solid-phase calculations. The gas-phase calculations were done with the same cutoff, but with a single *k* point (Γ point) and using a large $(20\ Å)^3$ supercell that mimics a single molecule in vacuum. Throughout the QE calculations, we use the PBE functional.[77] All calculations were done including van der Waals interaction (D3BJ dispersion), which is expected to be of particular relevance for the gas-phase structures.[68] The calculated spectra have been aligned with respect to the copper K-edge of the experimental spectra. The line width is chosen to be energy-dependent, rising arctan-like from 0.2 at 8975 eV to 2.0 at 8940 eV.[81] The broadening used in the calculations thus follows qualitatively the trend in the experimental spectra but is chosen to be somewhat smaller, in order to prevent it from masking the fine structure of the simulations.

Materials. The complexes $[Cu^I(DMEGqu)_2](PF_6)$ and $[Cu^{II}(DMEGqu)_2](OTf)_2{\cdot}MeCN$ were prepared according to a literature procedure.[56]

RESULTS AND DISCUSSION

HERFD-XANES Measurements. Two different counterions, PF_6^- and OTf^-, were used during crystallization of the copper(I) and copper(II) species, respectively.[56] The resulting key geometric parameters are given in Table 1; the unit cells and

Table 1. Geometric Parameters of the Two Complexes (Obtained from X-ray Diffraction)

	$[Cu^I(DMEGqu)_2]PF_6$	$[Cu^{II}(DMEGqu)_2](OTf)_2{\cdot}MeCN$[a]
Bond Length [Å]		
$Cu-N_{imine,gua}$	2.113(2), 2.134(2)	1.978(3), 1.998(3)
$Cu-N_{qu}$	1.981(2), 1.959(2)	1.986(3), 1.981(3)
$C_{gua}-N_{imine,gua}$	1.302(3), 1.309(3)	1.347(4), 1.342(4)
$C_{gua}-N_{amine,gua}$	1.361(3), 1.366(3)	1.325(4), 1.341(4)
	1.352(3), 1.357(3)	1.324(4), 1.346(4)
Chelate Angle [deg]		
N−Cu−N	81.9(1), 81.8(1)	81.8(1), 82.7(1)
Structure Factor		
$\tau_4 = \frac{360^\circ - (\alpha+\beta)}{141}$	0.57	0.36
Torsion Angle (deg)		
$\angle(C_{gua}N_3, CuN_2)$	44.2, 52.6	56.6, 60.4
$\angle(CuN_2, CuN'_2)$	63.1	42.2

[a]Here, two different molecules are present in the asymmetric unit.

molecular structures of $[Cu^I(DMEGqu)_2]^+$ and $[Cu^{II}(DMEGqu)_2]^{2+}$ in the solid state are compared in Figure 1. The unit cell of the copper(I) species consists of two molecules plus *two* counterions (PF_6^-), whereby the arrangement of the two molecules shows inversion symmetry (cf. Figure 1, left). For copper(II), the molecular crystal structure is more complex and consists of *four* molecules plus *eight* OTf^- counterions plus four acetonitrile molecules (cf. Figure 1, right).

As previously shown for $[Cu(tmeda)_2]^+$ (tmeda = tetramethylethylenediamine), one would expect a tetrahedral geometry for copper(I) complexes,[82] whereas the corresponding copper(II) system[83] is expected in a square-planar fashion. The DMEGqu complexes in this study exhibit geometries between these two extremes. The τ_4 parameter can be used to describe the geometry of a 4-fold coordination. By definition, ideal tetrahedral sites show a value of $\tau_4 = 1$ and square-planar sites $\tau_4 = 0$.[84] This was shown previously for related compounds,[7] and similar values are obtained.

The copper(I) complex $[Cu^I(DMEGqu)_2](PF_6)$ is characterized by a value of 0.57, indicative of a strongly distorted tetrahedron. The copper(II) complex $[Cu^{II}(DMEGqu)_2](OTf)_2{\cdot}MeCN$ shows a smaller value of 0.36. An alternative measure is given by the angle between the two chelate planes (90° = tetrahedron and 0° = square planar), which adopts values of 63° in the $[Cu^I(DMEGqu)_2]^+$ cation and 42° for $[Cu^{II}(DMEGqu)_2]^{2+}$, indicating a twist of about 20° upon oxidation.[56]

Figure 2 compares the conventional XANES spectra recorded in transmission with the HERFD-XANES spectra. The latter ones are obtained using a focusing Johann-type spectrometer with spherically bent analyzer crystals.[23,85] The energy of the

DOI: 10.1021/acs.inorgchem.6b01704
Inorg. Chem. 2016, 55, 11694−11706

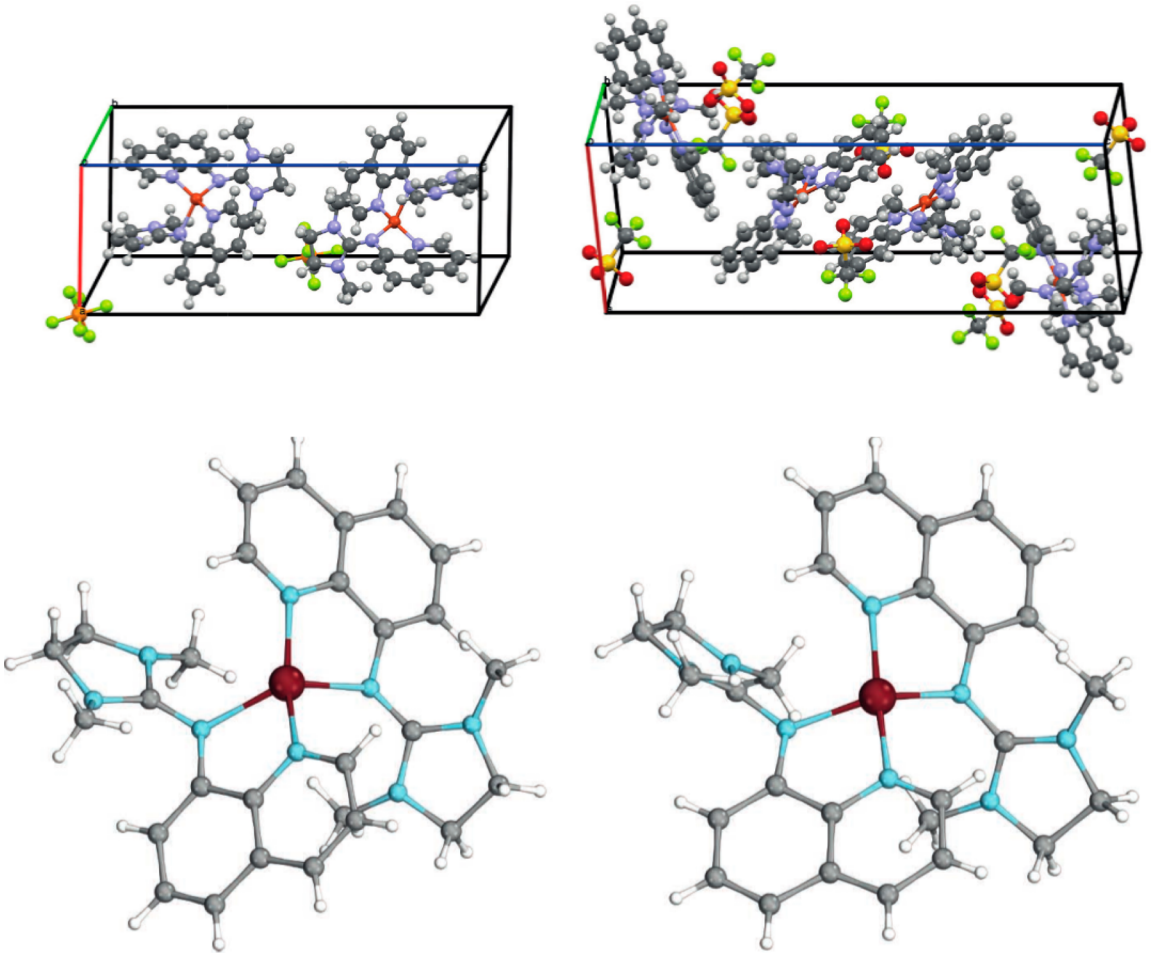

Figure 1. (Experimental) Unit cells of the complete molecular crystals (top) of $[Cu^{I}(DMEGqu)_2](PF_6)$ (triclinic, left) and $[Cu^{II}(DMEGqu)_2](OTf)_2 \cdot MeCN$ (triclinic, right) including the counterions. For the sake of clarity, enlarged structures of the cationic sites are shown below.[56]

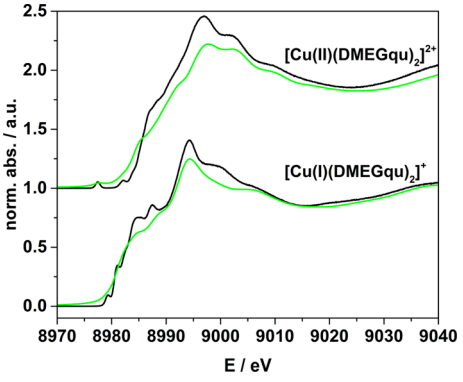

Figure 2. Comparison of the conventional (green) and high-resolution (black) XANES spectra taken for the same samples of $[Cu^{I}(DMEGqu)_2](PF_6)$ and $[Cu^{II}(DMEGqu)_2](OTf)_2 \cdot MeCN$ molecular crystals.

analyzer crystals is fixed at a certain value, and its intensity is recorded while the incident beam energy is swept over the absorption edge. These measurements follow the approach originally introduced by Hämäläinen et al.[86] as high-resolution fluorescence excitation in order to obtain lifetime-broadening-removed XANES spectra. Carra et al.[87] and Loeffen et al.[88] pointed out that this method is not strictly yielding lifetime-broadening-removed spectra. However, Tanaka et al.[89] showed that, under certain circumstances, the high-resolution excitation spectra are essentially identical with conventionally obtained XANES spectra but with much higher resolution and are thus called HERFD-XANES. Most important, the emitted photon energy has to correspond to a peak position in the fluorescent spectrum. Another core criterion is that off-diagonal elements representing nonlocal states are not present in the RIXS planes (cf. the Supporting Information) because they would lead to artifacts in the HERFD-XANES spectra. When this technique is applied, a tremendous increase in the resolution is observed,[25] as proven in Figure 2, whereby the degree of resolved fine structure is particularly obvious for the copper(I) complex. The benefit of high-energy-resolution-fluorescence detection is 3-fold: (i) the experimental background is nearly eliminated; (ii) the prepeak, if present, of the copper(II) complex is significantly better resolved, and (iii) the XANES fine structure is impressively sharpened but obviously to different extents.

While the first point is more or less only relevant for a better analysis of the prepeak intensities, the latter two points offer further valuable information on the investigated species: The 4-fold coordination can be identified by comparing the preedge intensity and general spectral shape to those in earlier studies.[90] Also, the influence of the oxidation state on the edge position is easily recognized: The edge of copper(II) is shifted by 3 eV with respect to copper(I). Most remarkably, the spectra, especially for the copper(I) case, reveal a detailed fine structure in the edge. In other words, the HERFD-XANES measurements yield richer spectral information compared to conventional measurements,

DOI: 10.1021/acs.inorgchem.6b01704
Inorg. Chem. 2016, 55, 11694−11706

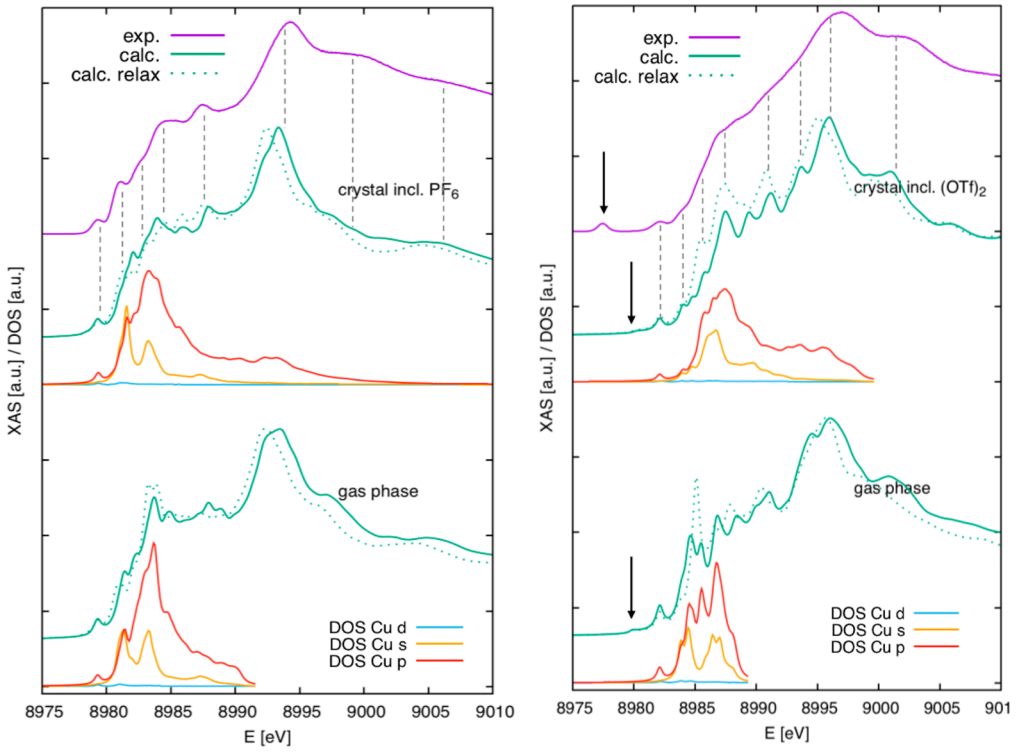

Figure 3. Comparison of the experimental copper(I) (left) and copper(II) (right) XAS spectra with theoretical PAW-XAS spectra calculated for the experimental crystal structures (solid green lines): (i) for a periodic molecular crystal including the counterions PF_6^- and OTf^-, respectively (top); (ii) for charged isolated molecules, i.e., for the gas phase (bottom). For further comparison, calculated spectra for the self-consistently relaxed structures are also indicated by dotted lines. Vertical dashed lines serve as guides for the eyes. For copper(II), the prepeak is indicated by arrows. The further curves describe the projected DOS.

which allows for a more detailed comparison to theoretical calculations, e.g., a more accurate assignment of the underlying transitions. As already mentioned in the Introduction, the prepeak region is best described by TD-DFT, while above the Fermi level, the continued-fraction approach describes the measured data very well. This will be demonstrated in the following sections.

DFT Simulations of XANES Spectra. *I. PAW-XAS Results.* In order to get an overview and an understanding of the general shape of the XAS spectra, we start our DFT simulation with the continued-fraction PAW-XAS method. The multiprojector GIPAW approach is able to describe the XAS spectrum in a broad energy range up to 30 eV and more above the copper K-edge, as demonstrated in Figure 3. Especially in the case of the copper(I) complex, the agreement is quite impressive if a periodic molecular crystal including the PF_6^- counterions is modeled (green curves in Figure 3, top): All peaks and shoulders are present and predicted at reasonably correct energies. For the copper(II) complex, in particular in the region 5−15 eV above the edge, the agreement is less obvious because the resolved experimental features are not as pronounced as those in the copper(I) case. Here, an improved agreement between the experiment and theory can be enforced by increasing the line width of the calculated spectra by a factor of 2. On the basis of the presently available data, we speculate that the larger unit cell for the copper(II) provides more spatial degrees of freedom and is potentially more easily affected by thermal vibrations and, consequently, by an enhanced thermal broadening of the spectra.

It is noteworthy that all of the PAW-XAS spectra are obtained while explicitly taking into account occupied states exclusively. Thanks to the projectors and the Lanzcos recursion scheme,[44−46] we can profit from the completeness relationship of an infinite quantum mechanical basis set by substituting (infinite) sums over empty states with (finite) sums over occupied states. In fact, additional calculations for the projected density of states (DOS) reveal that 420 empty states are distributed over a limited energy range of about 10 eV; see also the base lines in Figure 3. To cover the full energy range, several tens of thousands empty states would be required.

We further note that as good as possible agreement with the global shape of the experimental spectra is generally obtained by simulations that are based on the complete unit cell of the molecular crystal, taking also into account the counterions explicitly, either by using the experimental crystal structure from single-crystal X-ray diffraction (cf. Figure 1 and Table 1) or by using structures relaxed within DFT, i.e., as obtained from minimizing the Hellmann−Feynman forces within the molecular crystals. By the latter approach, the features of the far-edge part of the spectrum are slightly red-shifted toward the edge step, but in parallel some near-edge features are better described (see the dotted lines in Figure 3). This is, in particular, true for the copper(I) species and the shape and height of the characteristic shoulder at 8981 eV (2 eV above the edge), which originates from strong metal-to-ligand charge-transfer (MLCT) Cu 1s → C 2p, N 2p transitions.

When modeling the corresponding gas-phase species, i.e., the ionized isolated molecules without counterions, most features of the spectra are reproduced, but the relative intensity of some peaks is inverted in comparison to the experiment, in particular in the region 2−6 eV above the copper K-edge, where the Cu 1s → 4p transitions are strongly overestimated in the gas-phase modeling, in particular for the copper(II) case. Finally, the

DOI: 10.1021/acs.inorgchem.6b01704
Inorg. Chem. 2016, 55, 11694−11706

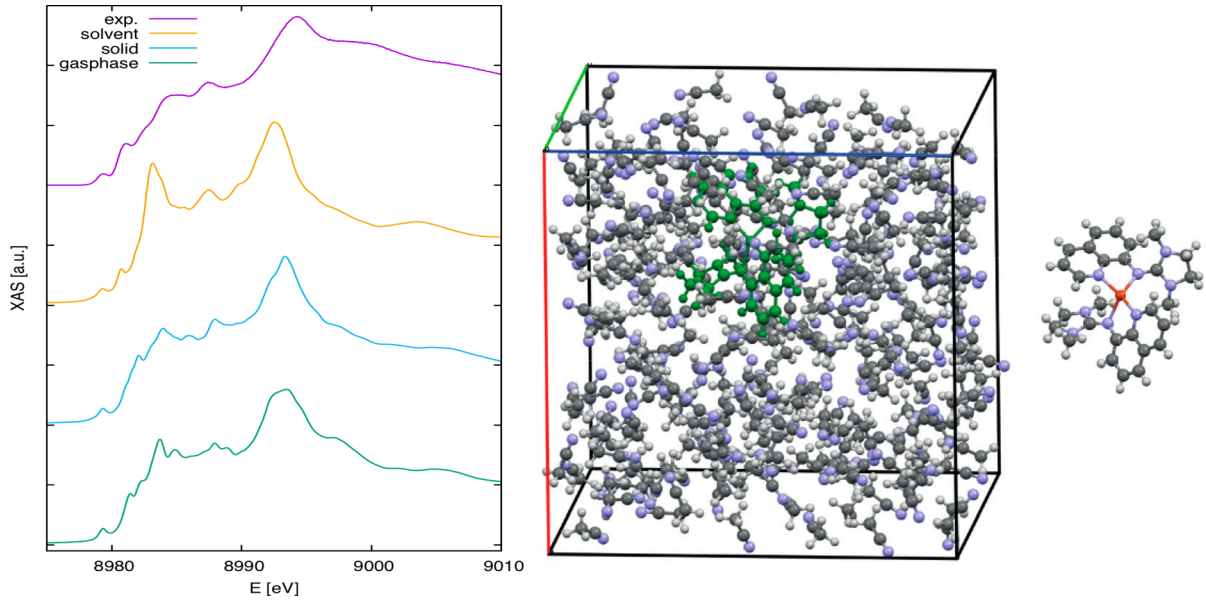

Figure 4. DFT-calculated XAS spectra for the $[Cu^{I}(DMEGqu)_2]^+$ species in acetonitrile (left, yellow line), modeled within a large, $25.7 \times 25.7 \times 25.7$ A^3 supercell (right) containing the copper(I) complex itself (green, colored besides) and 231 solvent molecules (in total 1452 atoms).

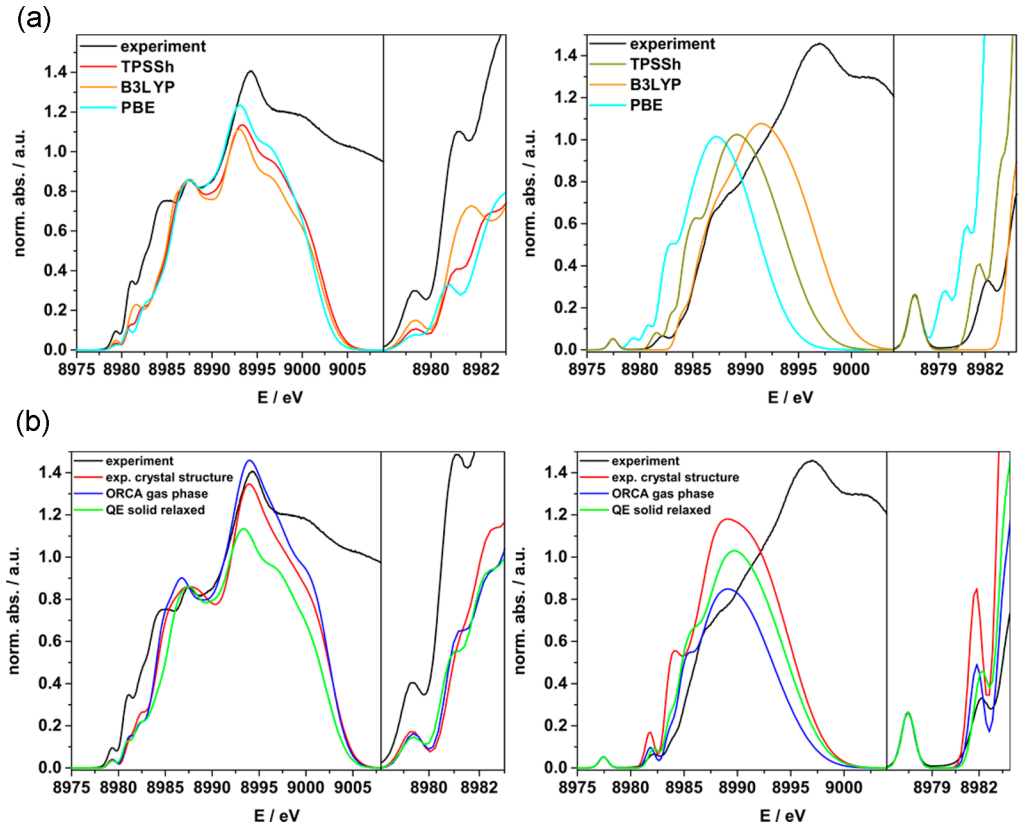

Figure 5. (a) Comparison of the TD-DFT-calculated copper(I) (left) and copper(II) (right) spectra using different XC functionals for the QE-relaxed solid structure. For copper(I), the intensity of the spectra is normalized to the intensity of the 8987 eV peak; for copper(II), it is normalized to that of the prepeak at 8977.5 eV. (b) Calculated XANES spectra (TD-DFT with the TPSSh functional) for DFT-relaxed structures (gas phase and molecular crystal) and for the experimental crystal structure in comparison to the experimental spectrum. For copper(I) (left), the intensity of the spectra is normalized to the intensity of the 8987 eV peak; for copper(II) (right), it is normalized to that of the prepeak at 8977.5 eV. Transitions into 120 and 250 empty states have been used for copper(I) and copper(II), respectively.

prepeak features caused by 1s → LUMO transitions are not properly described in the continued-fraction approach. The intensity of the prepeak at 8977.45 eV and its distance to the edge is considerably underestimated. The latter is mainly related to the common underestimation of the highest occupied molecular orbital (HOMO)−LUMO gaps if using semilocal XC functionals. Note that, for the near- and far-edge regions, related to transitions into more delocalized empty states, this problem plays

DOI: 10.1021/acs.inorgchem.6b01704
Inorg. Chem. 2016, 55, 11694−11706

a minor role. For a more detailed quantitative discussion of the prepeak, however, we refer to the TD-DFT calculations described below, where, in particular, the influence of the used XC functional is thoroughly investigated.

It has to be noted that, strictly speaking, the modeling of isolated molecules does not correspond to the experimental situation, where XAS is performed either on molecular crystals (solid state) or on molecular species in solution. Similar to the solid state, also in solution the interaction with the neighboring solvent molecules is able to influence the XAS spectra significantly. To illustrate this, we have performed additional calculations for the $[Cu^{I}(DMEGqu)_2]^+$ species in an acetonitrile (C_2H_3N) solution. For this purpose, a copper(I) complex has been modeled in a large supercell containing 231 solvent molecules equivalent to a 78 mM concentration of solution (see Figure 4). In a first step, the atomic positions of the copper(I) complex are kept fixed, while the distribution of the solvent molecules is optimized using molecular dynamics. Afterward, within such an optimized solvent environment, the copper(I) complex is allowed to relax freely. For the resulting structure, we calculate the copper K-edge XAS spectrum. Again a quite good agreement with the results of the solid-state simulation is obtained for large parts of the spectrum (cf. Figure 4, left). The peak at 8983 eV, however, appears to be considerably overestimated, similar to the relaxed gas-phase geometry, but even more pronounced (cf. Figure 3, bottom, left). The intensity of this peak, which is mainly characterized by transitions into the ligand π^* system with a predominant amount of C 2p orbitals (for further details, see the next section), depends very sensitively on the microscopic details of the solvent environment. This will result (i) in effectively reduced intensities in statistical ensembles as in the experiment and (ii) a considerably larger temperature dependence of the XAS spectra as in the case of the solid state (molecular crystals).

Obviously, precise modeling of the molecules in solution and simulation of their XAS spectra are rather cumbersome because they require statistical averaging over a large ensemble of structures. Here, the so-called gas-phase modeling of isolated molecules (within reasonable geometries) actually provides an efficient alternative, which will also be used in the TD-DFT calculations described below.

II. TD-DFT Results. Usually the intensity of a prepeak is used to adjust the TD-DFT-derived XAS spectra to the experimental spectra. For copper(II), this leads to an adequate relationship between the various spectra (see, e.g., Figure 5a, right). In the copper(I) case with a completely filled $3d^{10}$ shell, however, there is no such classical prepeak. Using the first peak at the copper K-edge instead is not reliable because its intensity depends strongly on the technical details of the theoretical description (e.g., the choice of the XC functional; cf. Figure 5a, left). Thus, it does not provide a reliable global reference. Here, we use the peak around 8987 eV as an alternative. Its intensity as well as its energetic position does not depend on the DFT functional, and the latter agrees nicely with the experimental one.

a. Influence of the Geometry. The relationship between the molecular structure and simulated spectra inferred from the continued-fraction approach is largely confirmed by TD-DFT calculations: The near-edge regions seem to be described slightly better when the DFT-relaxed structures are used instead of the experimental ones. This can be clearly seen in the case of the copper(II) species by analyzing the characteristic shoulder above 8985 eV. Figure 5b (right) shows (using the all-in-all best-performing TPSSh functional; cf. Figure 5a) that its shape is best reproduced for the fully relaxed crystal structure. At this point, it is not clear if this is really due to changes in the crystal structure, e.g., increased C−H bond lengths, or due to some kind of error cancellation within gas-phase modeling. Notably, for copper(II), the torsion angle between the two CuN_2 planes in the first coordination shell, a quantity that characterizes the entatic state of the complexes used for this study, is basically the same for the crystal structure relaxed within DFT-PBE and the relaxed gas-phase geometry obtained using the TPSSh functional. It becomes, however, obvious that the self-consistently relaxed gas-phase geometries provide no valid starting point for simulation of the X-ray spectra: The symmetry of the resulting structures is considerably overestimated; e.g., the Cu−N distances become pairwise identical (see Tables 2 and 3). In other words, the structures lose their characteristic asymmetry. With HERFD-XANES being a local method, the Cu−N distances are important as well, besides the torsion angle between the two CuNN planes. Unique shifts of all Cu−N distances (as expected for the bond length overestimating the PBE functional[65,67]) lead only to an energy shift of the whole spectra. The asymmetry within the two chemically equivalent $Cu-N_{qu}$ and $Cu-N_{imine,gua}$ distances, in contrast, leads to the characteristic splittings of the main peaks in the near-edge region, contributing substantially to the shape of the spectra.

Table 2. Geometric Parameters of the Copper(I) Structures Derived from Gas-Phase Optimization for Two Different DFT Functionals (TPSSh and PBE), from a Relaxation of the Molecular Crystal (Solid) and the Experimental Crystal Structure (from X-ray Diffraction) Itself

copper(I)	exptl crystal structure	gas-phase TPSSh	gas-phase PBE	solid relaxed PBE
τ_4	0.57	0.67	0.65	0.62
$Cu-N_{qu}$	1.981(2), 1.959(2)	1.973, 1.973	2.017, 2.017	2.025, 1.994
$Cu-N_{imine,gua}$	2.113(2), 2.134(2)	2.110, 2.109	2.181, 2.182	2.098, 2.098
$\angle CuN_2/CuN'_2$	63.1	76.6	76.6	69.6

Table 3. Geometric Parameters of the Copper(II) Structures Derived from Gas-Phase Optimization for Two Different DFT Functionals (TPSSh and PBE), from a Relaxation of the Molecular Crystal (solid) and the Experimental Crystal Structure (from X-ray Diffraction) Itself

copper(II)	exptl crystal structure	gas-phase TPSSh	gas-phase PBE	solid relaxed PBE
τ_4	0.36	0.43	0.47	0.46
$Cu-N_{qu}$	1.986(3), 1.981(3)	1.973, 1.972	2.027, 2.026	2.021, 2.008
$Cu-N_{imine,gua}$	1.978(3), 1.998(3)	1.967, 1.967	2.065, 2.066	2.033, 1.999
$\angle CuN_2/CuN'_2$	42.2	45.6	51.6	45.8

b. Influence of XC Functionals. Out of the functionals probed here, TPSSh performs all-in-all best concerning the modeling of the XANES spectra. Taking also the kinetic energy of the orbitals into account, this meta-hybrid functional with a moderate amount of Hartree−Fock (HF) exchange (10% in comparison to 25% in B3LYP) has been frequently reported to describe the structural and electronic properties of similar 3d transition-metal-including complexes.[7,66,67] We found that the absolute energies, i.e., the position of the copper K-edges, are generally closer to the experiment for all hybrid calculations. This can be

DOI: 10.1021/acs.inorgchem.6b01704
Inorg. Chem. 2016, 55, 11694−11706

explained with the addition of HF exchange reducing the self-interaction error and therefore giving higher accuracy for strongly localized core states as well as for the Cu 3d levels and, thus, for the corresponding core−excited state transitions.[32] Even more important, the energy splitting between the prepeak and the following features for the copper(II) species is too small for the nonhybrid functionals throughout all calculated spectra. It is noteworthy that this splitting is too small even for the TPSSh functional that contains rather moderate 10% exact exchange. The position of the prepeak becomes even worse (now too far away from the copper K-edge) for standard hybrid functionals like B3LYP. This kind of overcorrection, however, can be fixed by adjusting the fraction of HF exchange. In the case of copper(II), 12.5% HF exchange was needed to achieve the correct splitting in the preedge region (additional spectra provided in the Supporting Information), whereas for copper(I), the HF exchange did not show a significant influence, as can be seen in Figure 5b for the two spectra calculated with B3LYP (25% HF) and TPSSh (10% HF). We attribute this substantial difference to the electron configuration being paramagnetic $3d^9$ in the copper(II) case and diamagnetic closed-shell d^{10} for copper(I), which renders the concomitant influence of the exchange interaction less significant. In the following sections, only the TPSSh functional results will be discussed for the TD-DFT calculations.

c. Comparison with the Experiment. We start a more detailed discussion of the two different complexes with the copper(II) compound $[Cu^{II}(DMEGqu)_2](OTf)_2{\cdot}MeCN$, which, thanks to the open-shell $3d^9$ configuration, gives rise to the aforementioned distinct prepeak. The measured HERFD-XANES spectra (cf. Figures 2 and 5a,b) locate this prepeak at 8977.45 eV. Our TD-DFT calculations reveal a 1s orbital to LUMO transition underneath this peak. The spatial distribution of the β-LUMO is shown in Figure 6 and consists mostly (>55%)

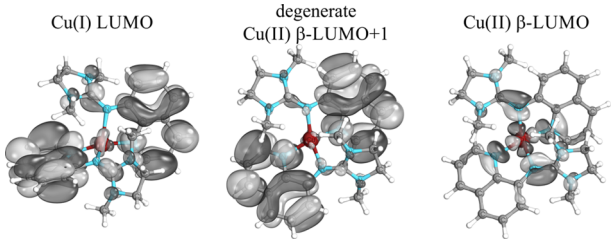

Figure 6. Comparison of the acceptor orbital (LUMO) related to the first transition peak in the calculated copper(I) spectra (left) and the degenerate β-LUMO+1/β-LUMO+2 of the copper(II) calculation (middle); acceptor orbital (β-LUMO) of the prepeak transition calculated for the copper(II) species (right).

of Cu 3d orbitals (detailed contributions are provided in the Supporting Information). A symmetry-dependent admixture of Cu p as well as p orbitals of the nitrogen and carbon ligands allows for a dipole transition that leads to a significantly enlarged intensity compared to a pure 1s → 3d transition. Nevertheless, the quadrupole (1s → 3d) transition still accounts for as much as 25% intensity. The following feature at 8982 eV is mainly characterized by transitions in the ligand π^* system with a predominant amount of C 2p orbitals. The next intense feature in the edge above 8985 eV can be assigned to a 1s → 4p + LMCT shakedown (multielectron) transition, similar to that reported previously for square-planar copper(II) complexes.[91] At higher energies, the localized and finite character of the basis set used for the TD-DFT calculations prevents the reproduction of spectral features. Additional multiscattering effects, thus, cannot be considered within TD-DFT.[92]

As already mentioned above, the copper(I) spectrum of $[Cu^{I}(DMEGqu)_2](PF_6)$ (Figure 5a,b, left) shows no prepeak because the $3d^{10}$ configuration does not allow for 1s → 3d transitions. The LUMO for the copper(I) species is shown in Figure 6 (left) and consists mostly of ligand π^* orbitals. These features around 8980 eV can accordingly be assigned to MLCT transitions. A closer look reveals that this calculated feature is of the same character as that in the copper(II) case but shifted to lower energies because of the smaller ionization threshold in copper(I), i.e., the influence of the nuclear charge on the orbital energies. The LUMO of the copper(I) case (Figure 6, left) is indeed very similar to the degenerate β-LUMO+1/β-LUMO+2 (Figure 6, middle) in the copper(II) case. These assignments strengthen the MLCT assignment.[33,93] The copper(I) spectra show a characteristic, very intense 1s → 4p transition visible as a shoulder. This feature is shifted to higher energies for copper(II); it is, therefore, often hidden under the edge.

d. Sensitivity to Structural Changes. To further elucidate the effect of geometrical distortions on the XANES spectra (as, e.g., relevant in entatic states), we also calculated spectra for *constrained* tetrahedral ($\angle CuN_2/CuN_2' = 90°$) and square-planar ($\angle CuN_2/CuN_2' = 0°$) geometries. For this purpose, the values of the N−Cu−N angles (except the two ligand chelate angles) were fixed, while otherwise relaxing the positions of all of the atoms of the cationic gas-phase molecules. Thereby, the $\angle CuN_2/CuN_2'$ angles were fixed to the mentioned 0°/90° values as well. This also results in a change of the bond lengths (see the Supporting Information), which has been described earlier,[65] but does not affect the value for the following discussion. The XANES spectra (Figure 7, left) calculated for the two resulting structures show clearly distinguishable prepeak intensities as well as significantly different intensities for the following preedge transitions. This can be explained by the changing amount of the p contribution to the acceptor orbital of the excitation in the XAS process. The square-planar case mimics an ideal quadrupole. Consequently, the prepeak is predominantly determined by the quadrupole term. No significant dipole contribution is found because in the LUMO there is no admixture of Cu p orbitals and only a little of the C and N p orbitals. Note that the contribution of the N p orbitals remains nearly constant and is, thus, not discussed further in this context. The tetrahedral coordination, in contrast, shows a maximum electric-dipole contribution (being responsible for more than 90% of the intensity). The LUMO in this case consists of 2% Cu 4p and 15% C 2p orbitals in conjunction with an amount of 45% Cu d. Figure 8 shows the orbital shape of the LUMOs; the orbital contributions for the different cases are listed in Table 4. A comparison of the shape and features of the calculated spectra confirms the importance of the $\angle CuN_2/CuN_2'$ angle. As expected, none of the extreme cases is able to reproduce the spectrum of the $[Cu^{II}(DMEGqu)_2](OTf)_2{\cdot}MeCN$ structure. Mixing, however, the spectra obtained for the two extreme angles of 0 and 90° with their respective ratios (51% tetrahedral and 49% square-planar, giving an angle of 45.84°; cf. Table 3) results in a spectrum that shows a good agreement with the actual spectrum of $[Cu^{II}(DMEGqu)_2](OTf)_2{\cdot}MeCN$, despite the tetrahedral and square-planar geometries being strongly constrained, i.e., providing hypothetical constructs. In Figure 7 (TD-DFT results), this is shown for the near-edge regime, and in Figure 9, right (PAW-XAS results), also for the far-edge region using the same mixing ratio

DOI: 10.1021/acs.inorgchem.6b01704
Inorg. Chem. 2016, 55, 11694−11706

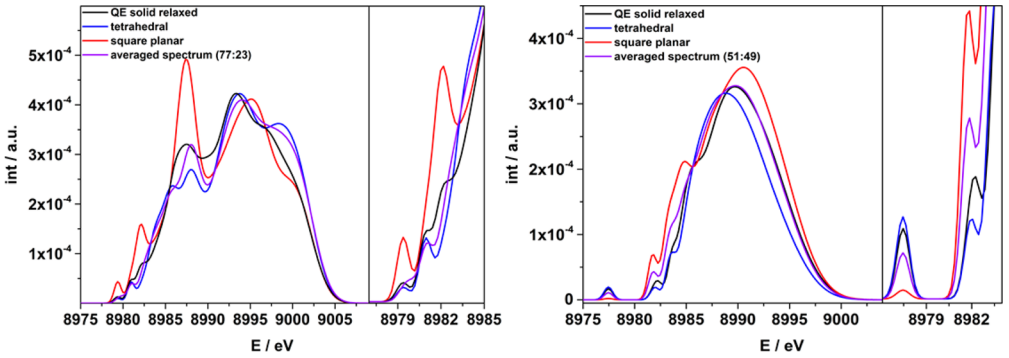

Figure 7. Comparison of the TD-DFT calculated spectra for the constrained square-planar and tetrahedral geometries for the copper(I) (left) and copper(II) (right) cases. Weighted-averaged spectra (77:23 and 51:49, respectively) and the spectra from a fully relaxed crystal geometry (QE solid relaxed) are also given. Right insets: zoom of the preedge regions.

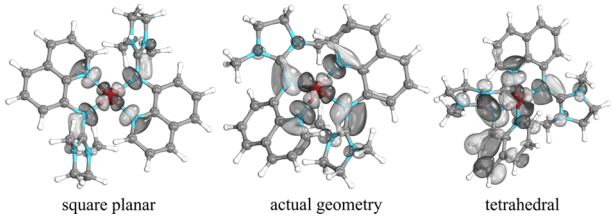

Figure 8. Spatial distribution of the β-LUMO orbitals for the three different copper(II) configurations, illustrating the increasing localization on the ligands with increasing tetrahedral distortion.

Table 4. s, p, and d Orbital Contributions (%) for Each LUMO of the Copper(II) Calculations Split into Fractions for Copper, Nitrogen, and Carbon

	Cu		N		C	
LUMO contributions	p	d	s	p	s	p
solid relaxed	2.3	55.0	2.9	20.7	0.0	6.9
square-planar	0.0	57.3	4.1	22.0	0.0	4.5
tetrahedral	2.0	45.1	1.1	21.9	0.0	15.5

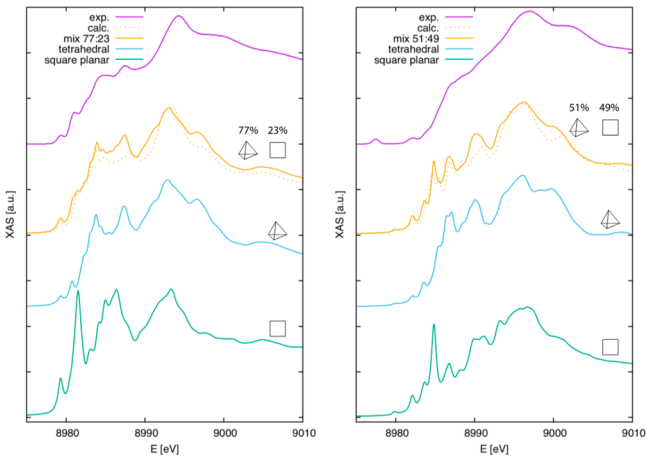

Figure 9. Theoretical XANES spectra for the copper(I) (left) and copper(II) (right) gas-phase molecules (PAW-XAS results) calculated for different geometries: for the constrained square-planar (green) and tetrahedral (blue) geometries and for the weighted mixtures of 77:23 for copper(I) and 51:49 for copper(II). For comparison, the spectra for the minimum total energy geometries are also indicated (dotted lines), and the experimental spectra (top) are also given again.

of 51:49. Here, the curve from mixing, i.e., more or less from averaging the constrained limits (solid line), follows nicely the curve calculated for the actual experimental geometry (dashed line); by this, it also agrees with the experimental HERFD-XANES spectrum. In addition, this procedure leads to a magnification of the prepeak, most clearly visible in the square-planar geometry.

For copper(I), the benefit of the mixing procedure is also significant (Figure 9, left). However, the tetrahedral contribution dominates the now clearly weighted superposition given by 77% (tetrahedral) and 23% (square-planar) relating to an angle of 69.59° (cf. Table 2). As a consequence, already the purely tetrahedral geometry reproduces the actual experimental spectrum of $[Cu^{I}(DMEGqu)_2](PF_6)$ for the high-energy transitions above 8982 eV. In this sense, for copper(I), the benefit of a square-planar admixture is restricted to the region close to the edge: In TD-DFT (Figure 7, left), the square-planar spectrum yields a too large energetic split-up between the first transitions. The tetrahedral limit, on the other hand, fits the preedge region quite well. The combination of both extremes again fits the features as well as in the copper(II) case.

SUMMARY AND CONCLUSION

Here HERFD-XANES spectroscopy is combined for the first time with the theoretical spectroscopy based on TD-DFT and the PAW-XAS approach in order to achieve a comprehensive description and understanding of the HERFD-XANES data. This combined approach was applied to provide a proof-of-principle for the investigation of small structural changes (e.g., entatic-state effects) in biomimetic geometrically constrained copper complexes. A Cu^{I}/Cu^{II} redox couple stabilized by a DMEGqu ligand served as an ideal case study: the 4-fold Cu−N coordination in both oxidation states deviates from the prototypical textbook cases, tetrahedral for copper(I) and square-planar for copper(II).

With the combination of TD-DFT and PAW-XAS, the rich information content in the HERFD-XANES spectra, ranging from the preedge signals, over the edge fine structure up to the first oscillations in the XAS coefficient after the edge step, can be fully utilized to characterize the structural and electronic changes when the copper oxidation state is changed from Cu^{I} to Cu^{II}. It thus will enable future high-resolution X-ray studies on the ET processes facilitated by ligand-induced geometry distortions. While the preedge peak is best described by TD-DFT because of its localized 1s → LUMO transitions, the local basis used in the TD-DFT calculations prevents a proper description of

DOI: 10.1021/acs.inorgchem.6b01704
Inorg. Chem. 2016, 55, 11694−11706

transitions at higher energies in the near-edge and, in particular, the far-edge region. Nevertheless, the range over which TD-DFT predicts spectral features with reasonable quality even in the rising edge region with its quasi-continuum states is astonishing and, to our knowledge, unprecedented: So far, TD-DFT has only been applied to predict preedge peaks, and no attempts were made to apply it to transitions beyond these energies.[92,94]

But still, starting with the rising edge, the PAW-XAS approach in the continued fraction is superior because (i) plane waves are ideally suited to describe the delocalized high-energy states and periodic systems such as the experimentally investigated molecular crystals, (ii) thanks to a multiprojector description, the Lanzcos recursion scheme, and (iii) by making use of completeness relation, the XANES spectra can be reasonably described for a broad energy range covering at least 30 eV. Although muffin-tin full multiple scattering and finite-difference-method approaches are more powerful to simulate spectra up to higher energies including the EXAFS region, the results here are the first to simulate XANES data using a full-electron approach that proves to be accurate enough to reproduce even the features in the HERFD-XANES spectra in terms of energy and intensity.

With both methods, the effect of geometrical distortion on the electronic structure in an entatic-state model, as reflected in the HERFD-XANES spectra of the molecular crystals, can be explained. In order to investigate the feasibility of the applied theoretical methods, different kinds of modeling were used in the theoretical spectral calculations: (i) periodic molecular crystals from the experimental single-crystal parameters as well as fully relaxed geometries and (ii) charged isolated gas-phase molecules. The PAW-XAS calculations based on the periodic molecular crystal (including the counterions) give slightly better results than simulations based on gas-phase molecules. The latter, however, still predict all transitions but with reduced accuracy concerning the peak intensities. The same trend is obtained in the TD-DFT calculations. Here, the TPSSh hybrid functional is found to yield best results, confirming recent findings from similar copper complexes.[65−68]

It could finally be shown that, for cases in which expensive theoretical calculations are *not* feasible, a simple fingerprint approach based on the linear combination XANES principle[95,96] can be used to identify the degree of internal, ligand-induced distortion by comparing experimental data with a weighted mixture of spectra calculated for hypothetical tetrahedral and square-planar structures of the same compound. This requires, of course, high-resolution experimental spectra that are available thanks to HERFD-XANES spectroscopy.

With these results, the way is paved for investigations on biomimetic complexes in situ, i.e., under biocatalytic conditions. Such systems are characterized by low concentrations and interfering solvent molecules. By additional comparative calculations, we have shown that the spectra of *individual* molecules in solution depend strongly on the microscopic details of the solvent environment. The statistical ensembles investigated in the experiments, thus, seem to be explained in a more reliable way by modeling gas-phase molecules. However, further detailed studies are necessary to confirm this suggestion for biomimetic complexes in low-concentrated solution in general. By using hard X-rays in HERFD-XANES measurements, which are conducted in fluorescence geometry and with high incoming fluxes, the electronic states and connectively the geometric structure can be determined under such conditions. Moreover, making use of time-resolved experiments at synchrotrons or even free electron lasers,[97−100] the ET reactions of the entatic state and type-zero model complexes can be investigated by means of the changes in the orbital contributions to the HERFD-XANES spectra. We finally conclude that HERFD-XANES in combination with computational modeling opens up new opportunities for the investigation of ET processes in chemistry.

■ ASSOCIATED CONTENT

Supporting Information

The Supporting Information is available free of charge on the ACS Publications website at DOI: 10.1021/acs.inorgchem.6b01704.

RIXS planes, calculated spectra of additional geometries, and acceptor orbital contributions of selected transitions and geometric parameters of the geometries used in the calculations (PDF)

■ AUTHOR INFORMATION

Corresponding Authors

*E-mail: uwe.gerstmann@uni-paderborn.de (U.G.).
*E-mail: matthias.bauer@uni-paderborn.de (M.B.).

Author Contributions

[§]These authors contributed equally to this work and should therefore be acknowledged as joint first authors.

Notes

The authors declare no competing financial interest.

■ ACKNOWLEDGMENTS

The ESRF is acknowledged for a provision of beamtime. We thank Dr. Mauro Rovezzi for assistance during the measurements. The Deutsche Forschungsgemeinschaft is acknowledged for financial support (Grant FOR1405). Generous grants of computer time at the Paderborn Center for Parallel Computing PC[2] and the HLRS Stuttgart are gratefully acknowledged.

■ REFERENCES

(1) Solomon, E. I.; Hadt, R. G. Recent advances in understanding blue copper proteins. *Coord. Chem. Rev.* **2011**, *255*, 774−789.
(2) Hosseinzadeh, P.; Marshall, N. M.; Chacón, K. N.; Yu, Y.; Nilges, M. J.; New, S. Y.; Tashkov, S. A.; Blackburn, N. J.; Lu, Y. Design of a single protein that spans the entire 2-V range of physiological redox potentials. *Proc. Natl. Acad. Sci. U. S. A.* **2016**, *113*, 262−267.
(3) Lancaster, K. M.; DeBeer George, S.; Yokoyama, K.; Richards, J. H.; Gray, H. B. Type-zero copper proteins. *Nat. Chem.* **2009**, *1*, 711−715.
(4) Comba, P.; Kerscher, M. Computation of structures and properties of transition metal compounds. *Coord. Chem. Rev.* **2009**, *253*, 564−574.
(5) Rorabacher, D. B. Electron Transfer by Copper Centers. *Chem. Rev.* **2004**, *104*, 651−697.
(6) Gray, H. B.; Malmström, B. G.; Williams, R. J. P. Copper coordination in blue proteins. *JBIC, J. Biol. Inorg. Chem.* **2000**, *5*, 551−559.
(7) Hoffmann, A.; Binder, S.; Jesser, A.; Haase, R.; Flörke, U.; Gnida, M.; Salomone-Stagni, M.; Meyer-Klaucke, W.; Lebsanft, B.; Grünig, L. E.; Schneider, S.; Hashemi, M.; Goos, A.; Wetzel, A.; Rübhausen, M.; Herres-Pawlis, S. Catching an Entatic State-A Pair of Copper Complexes. *Angew. Chem., Int. Ed.* **2014**, *53*, 299−304.
(8) Comba, P. Coordination compounds in the entatic state. *Coord. Chem. Rev.* **2000**, *200−202*, 217−245.
(9) Hancock, R. D.; Martell, A. E. Ligand design for selective complexation of metal ions in aqueous solution. *Chem. Rev.* **1989**, *89*, 1875−1914.
(10) Knapp, S.; Keenan, T. R.; Zhang, X.; Fikar, R.; Potenza, J. A.; Schugar, H. J. Nearly tetrahedral 1:2 complexes of copper(I), copper(II), nickel(II), cobalt(II), and zinc(II) with 2,2′-bis(2-imidazolyl)biphenyl. *J. Am. Chem. Soc.* **1987**, *109*, 1882−1883.

DOI: 10.1021/acs.inorgchem.6b01704
Inorg. Chem. 2016, 55, 11694−11706

(11) Comba, P.; Kerscher, M.; Roodt, A. Slow Electron Self-Exchange in Spite of a Small Inner-Sphere Reorganisation Energy ? The Electron-Transfer Properties of a Copper Complex with a Tetradentate Bispidine Ligand. *Eur. J. Inorg. Chem.* **2004**, *2004*, 4640−4645.
(12) Xie, B.; Elder, T.; Wilson, L. J.; Stanbury, D. M. Internal Reorganization Energies for Copper Redox Couples: The Slow Electron-Transfer Reactions of the [Cu II/I (bib) 2] 2+/+ Couple. *Inorg. Chem.* **1999**, *38*, 12−19.
(13) Chaka, G.; Sonnenberg, J. L.; Schlegel, B. H.; Heeg, M. J.; Jaeger, G.; Nelson, T. J.; Ochrymowycz, L. A.; Rorabacher, D. B. A Definitive Example of a Geometric "Entatic State" Effect: Electron-Transfer Kinetics for a Copper(II/I) Complex Involving A Quinquedentate Macrocyclic Trithiaether−Bipyridine Ligand. *J. Am. Chem. Soc.* **2007**, *129*, 5217−5227.
(14) Garcia, L.; Cisnetti, F.; Gillet, N.; Guillot, R.; Aumont-Nicaise, M.; Piquemal, J.-P.; Desmadril, M.; Lambert, F.; Policar, C. Entasis through Hook-and-Loop Fastening in a Glycoligand with Cumulative Weak Forces Stabilizing Cu I. *J. Am. Chem. Soc.* **2015**, *137*, 1141−1146.
(15) Dahl, E. W.; Szymczak, N. K. Hydrogen Bonds Dictate the Coordination Geometry of Copper: Characterization of a Square-Planar Copper(I) Complex. *Angew. Chem.* **2016**, *128*, 3153−3157.
(16) Comba, P. Strains and stresses in coordination compounds. *Coord. Chem. Rev.* **1999**, *182*, 343−371.
(17) Comba, P.; Schiek, W. Fit and misfit between ligands and metal ions. *Coord. Chem. Rev.* **2003**, *238*−*239*, 21−29.
(18) Comba, P.; Müller, V.; Remenyi, R. Interpretation of the temperature-dependent color of blue copper protein mutants. *J. Inorg. Biochem.* **2004**, *98*, 896−902.
(19) Bauer, M.; Bertagnolli, H. X-Ray Absorption Spectroscopy - the Method and Its Applications. *Methods in Physical Chemistry*; Wiley-VCH Verlag GmbH & Co. KGaA: Weinheim, Germany, 2012; pp 231−269.
(20) Haumann, M.; Liebisch, P.; Müller, C.; Barra, M.; Grabolle, M.; Dau, H. Photosynthetic O2 Formation Tracked by Time-Resolved X-ray Experiments. *Science* **2005**, *310*, 1019−1021.
(21) Dau, H.; Liebisch, P.; Haumann, M. X-ray absorption spectroscopy to analyze nuclear geometry and electronic structure of biological metal centers-potential and questions examined with special focus on the tetra-nuclear manganese complex of oxygenic photosynthesis. *Anal. Bioanal. Chem.* **2003**, *376*, 562−583.
(22) Bjornsson, R.; Delgado-Jaime, M. U.; Lima, F. A.; Sippel, D.; Schlesier, J.; Weyhermüller, T.; Einsle, O.; Neese, F.; DeBeer, S. Molybdenum L-edge XAS spectra of MoFe nitrogenase. *Z. Anorg. Allg. Chem.* **2015**, *641*, 65−71.
(23) Glatzel, P.; Bergmann, U. High resolution 1s core hole X-ray spectroscopy in 3d transition metal complexes - Electronic and structural information. *Coord. Chem. Rev.* **2005**, *249*, 65−95.
(24) Atkins, A. J.; Bauer, M.; Jacob, C. R. High-resolution X-ray absorption spectroscopy of iron carbonyl complexes. *Phys. Chem. Chem. Phys.* **2015**, *17*, 13937−13948.
(25) Bauer, M. HERFD-XAS and valence-to-core-XES: new tools to push the limits in research with hard X-rays? *Phys. Chem. Chem. Phys.* **2014**, *16*, 13827−13837.
(26) Bechstedt, F. *Many-Body Approach to Electronic Excitations*; Springer Series in Solid-State Sciences 181; Springer: Berlin, 2015.
(27) Shirley, E. L. Ab Initio Inclusion of Electron-Hole Attraction: Application to X-Ray Absorption and Resonant Inelastic X-Ray Scattering. *Phys. Rev. Lett.* **1998**, *80*, 794−797.
(28) Coriani, S.; Fransson, T.; Christiansen, O.; Norman, P. Asymmetric-lanczos-chain-driven implementation of electronic resonance convergent coupled-cluster linear response theory. *J. Chem. Theory Comput.* **2012**, *8*, 1616−1628.
(29) List, N. H.; Coriani, S.; Christiansen, O.; Kongsted, J. Identifying the Hamiltonian structure in linear response theory. *J. Chem. Phys.* **2014**, *140*, 224103.
(30) Peng, B.; Lestrange, P. J.; Goings, J. J.; Caricato, M.; Li, X. Energy-Specific Equation-of-Motion Coupled-Cluster Methods for High-Energy Excited States: Application to K -edge X-ray Absorption Spectroscopy. *J. Chem. Theory Comput.* **2015**, *11*, 4146−4153.
(31) Myhre, R. H.; Coriani, S.; Koch, H. Near-Edge X-ray Absorption Fine Structure within Multilevel Coupled Cluster Theory. *J. Chem. Theory Comput.* **2016**, *12*, 2633−2643.
(32) Besley, N. A.; Gilbert, A. T. B.; Gill, P. M. W. Self-consistent-field calculations of core excited states. *J. Chem. Phys.* **2009**, *130*, 124308.
(33) DeBeer George, S.; Petrenko, T.; Neese, F. Prediction of Iron K-Edge Absorption Spectra Using Time-Dependent Density Functional Theory †. *J. Phys. Chem. A* **2008**, *112*, 12936−12943.
(34) Roper, I. P. E.; Besley, N. A. The effect of basis set and exchange-correlation functional on time-dependent density functional theory calculations within the Tamm-Dancoff approximation of the x-ray emission spectroscopy of transition metal complexes. *J. Chem. Phys.* **2016**, *144*, 114104.
(35) Zhang, Y.; Mukamel, S.; Khalil, M.; Govind, N. Simulating Valence-to-Core X-ray Emission Spectroscopy of Transition Metal Complexes with Time-Dependent Density Functional Theory. *J. Chem. Theory Comput.* **2015**, *11*, 5804−5809.
(36) Onida, G.; Reining, L.; Rubio, A. Electronic excitations: Density-functional versus many-body Green's-function approaches. *Rev. Mod. Phys.* **2002**, *74*, 601−659.
(37) Wu, Q.; van Voorhis, T. Constrained Density Functional Theory and Its Application in Long-Range Electron Transfer. *J. Chem. Theory Comput.* **2006**, *2*, 765−774.
(38) Evangelista, F. A.; Shushkov, P.; Tully, J. C. Orthogonality Constrained Density Functional Theory for Electronic Excited States. *J. Phys. Chem. A* **2013**, *117*, 7378−7392.
(39) Derricotte, W. D.; Evangelista, F. A. Simulation of X-ray absorption spectra with orthogonality constrained density functional theory. *Phys. Chem. Chem. Phys.* **2015**, *17*, 14360−14374.
(40) Krewald, V.; Retegan, M.; Cox, N.; Messinger, J.; Lubitz, W.; DeBeer, S.; Neese, F.; Pantazis, D. A. Metal oxidation states in biological water splitting. *Chem. Sci.* **2015**, *6*, 1676−1695.
(41) Riefer, A.; Rauls, E.; Schmidt, W. G.; Eberhard, J.; Stoll, I.; Mattay, J. 2-Aminopyrimidine-silver(I) based organic semiconductors: Electronic structure and optical response. *Phys. Rev. B: Condens. Matter Mater. Phys.* **2012**, *85*, 165202.
(42) Chandrasekaran, P.; Stieber, S. C. E.; Collins, T. J.; Que, L., Jr.; Neese, F.; DeBeer, S. Prediction of high-valent iron K-edge absorption spectra by time-dependent Density Functional Theory. *Dalton Trans.* **2011**, *40*, 11070−11079.
(43) Lanczos, C. Solution of systems of linear equations by minimized iterations. *J. Res. Natl. Bur. Stand.* **1952**, *49*, 33−53.
(44) Haydock, R.; Heine, V.; Kelly, M. J. Electronic structure based on the local atomic environment for tight-binding bands. II. *J. Phys. C: Solid State Phys.* **1975**, *8*, 2591−2605.
(45) Walker, B.; Gebauer, R. Ultrasoft pseudopotentials in time-dependent density-functional theory. *J. Chem. Phys.* **2007**, *127*, 164106.
(46) Giannozzi, P.; Baroni, S.; Bonini, N.; Calandra, M.; Car, R.; Cavazzoni, C.; Ceresoli, D.; Chiarotti, G. L.; Cococcioni, M.; Dabo, I.; Dal Corso, A.; de Gironcoli, S.; Fabris, S.; Fratesi, G.; Gebauer, R.; Gerstmann, U.; Gougoussis, C.; Kokalj, A.; Lazzeri, M.; Martin-Samos, L.; Marzari, N.; Mauri, F.; Mazzarello, R.; Paolini, S.; Pasquarello, A.; Paulatto, L.; Sbraccia, C.; Scandolo, S.; Sclauzero, G.; Seitsonen, A. P.; Smogunov, A.; Umari, P.; Wentzcovitch, R. M. QUANTUM ESPRESSO: a modular and open-source software project for quantum simulations of materials. *J. Phys.: Condens. Matter* **2009**, *21*, 395502.
(47) Taillefumier, M.; Cabaret, D.; Flank, A.-M.; Mauri, F. X-ray absorption near-edge structure calculations with the pseudopotentials: Application to the K edge in diamond and α -quartz. *Phys. Rev. B: Condens. Matter Mater. Phys.* **2002**, *66*, 195107.
(48) Gougoussis, C.; Calandra, M.; Seitsonen, A. P.; Mauri, F. First-principles calculations of x-ray absorption in a scheme based on ultrasoft pseudopotentials: From α -quartz to high- T c compoun. *Phys. Rev. B: Condens. Matter Mater. Phys.* **2009**, *80*, 075102.
(49) Buczko, R.; Duscher, G.; Pennycook, S. J.; Pantelides, S. T. Excitonic Effects in Core-Excitation Spectra of Semiconductors. *Phys. Rev. Lett.* **2000**, *85*, 2168−2171.
(50) Gougoussis, C.; Rueff, J.-P.; Calandra, M.; d'Astuto, M.; Jarrige, I.; Ishii, H.; Shukla, A.; Yamada, I.; Azuma, M.; Takano, M. Multiple pre-

DOI: 10.1021/acs.inorgchem.6b01704
Inorg. Chem. 2016, 55, 11694−11706

edge structures in Cu K -edge x-ray absorption spectra of high- T c cuprates revealed by high-resolution x-ray absorption spectroscopy. *Phys. Rev. B: Condens. Matter Mater. Phys.* **2010**, *81*, 224519.
(51) Gaudry, E.; Cabaret, D.; Brouder, C.; Letard, I.; Rogalev, A.; Wilhlem, F.; Jaouen, N.; Sainctavit, P. Relaxations around the substitutional chromium site in emerald: X-ray absorption experiments and density functional calculations. *Phys. Rev. B: Condens. Matter Mater. Phys.* **2007**, *76*, 094110.
(52) Juhin, A.; Brouder, C.; Arrio, M.-A.; Cabaret, D.; Sainctavit, P.; Balan, E.; Bordage, A.; Seitsonen, A. P.; Calas, G.; Eeckhout, S. G.; Glatzel, P. X-ray linear dichroism in cubic compounds: The case of Cr 3 + in MgAl. *Phys. Rev. B: Condens. Matter Mater. Phys.* **2008**, *78*, 195103.
(53) Cabaret, D.; Mauri, F.; Henderson, G. S. Oxygen K -edge XANES of germanates investigated using first-principles calculations. *Phys. Rev. B: Condens. Matter Mater. Phys.* **2007**, *75*, 184205.
(54) Bunău, O.; Calandra, M. Projector augmented wave calculation of x-ray absorption spectra at the L 2, 3 edges. *Phys. Rev. B: Condens. Matter Mater. Phys.* **2013**, *87*, 205105.
(55) Juhin, A.; de Groot, F.; Vankó, G.; Calandra, M.; Brouder, C. Angular dependence of core hole screening in LiCoO2: A DFT+U calculation of the oxygen and cobalt K -edge x-ray absorption spectra. *Phys. Rev. B: Condens. Matter Mater. Phys.* **2010**, *81*, XX.
(56) Hoffmann, A.; Stanek, J.; Dicke, B.; Peters, L.; Wetzel, A.; Grimm-Lebsanft, B.; Jesser, A.; Bauer, M.; Gnida, M.; Meyer-Klaucke, W.; Rübhausen, M.; Herres-Pawlis, S. Implications of guanidine substitution on copper complexes as entatic state models. *Eur. J. Inorg. Chem.* **2016**, *2016*, 4731.
(57) Neese, F. The ORCA program system. *Wiley Interdiscip. Rev.-Comput. Mol. Sci.* **2012**, *2*, 73−78.
(58) DeBeer George, S.; Petrenko, T.; Neese, F. Time-dependent density functional calculations of ligand K-edge X-ray absorption spectra. *Inorg. Chim. Acta* **2008**, *361*, 965−972.
(59) DeBeer George, S.; Neese, F. Calibration of scalar relativistic density functional theory for the calculation of sulfur K-edge X-ray absorption spectra. *Inorg. Chem.* **2010**, *49*, 1849−1853.
(60) Neese, F. Prediction and interpretation of the 57Fe isomer shift in Mössbauer spectra by density functional theory. *Inorg. Chim. Acta* **2002**, *337*, 181−192.
(61) Schäfer, A.; Horn, H.; Ahlrichs, R. Fully optimized contracted Gaussian basis sets for atoms Li to Kr. *J. Chem. Phys.* **1992**, *97*, 2571.
(62) Schäfer, A.; Huber, C.; Ahlrichs, R. Fully optimized contracted Gaussian basis sets of triple zeta valence quality for atoms Li to Kr. *J. Chem. Phys.* **1994**, *100*, 5829−5835.
(63) Weigend, F.; Ahlrichs, R. Balanced basis sets of split valence, triple zeta valence and quadruple zeta valence quality for H to Rn: Design and assessment of accuracy. *Phys. Chem. Chem. Phys.* **2005**, *7*, 3297−3305.
(64) Staroverov, V. N.; Scuseria, G. E.; Tao, J.; Perdew, J. P. Comparative assessment of a new nonempirical density functional: Molecules and hydrogen-bonded complexes. *J. Chem. Phys.* **2003**, *119*, 12129−12137.
(65) Jesser, A.; Rohrmüller, M.; Schmidt, W. G.; Herres-Pawlis, S. Geometrical and optical benchmarking of copper guanidine-quinoline complexes: Insights from TD-DFT and many-body perturbation theory. *J. Comput. Chem.* **2014**, *35*, 1−17.
(66) Hoffmann, A.; Grunzke, R.; Herres-Pawlis, S. Insights into the influence of dispersion correction in the theoretical treatment of guanidine-quinoline copper(I) complexes. *J. Comput. Chem.* **2014**, *35*, 1943−1950.
(67) Hoffmann, A.; Rohrmüller, M.; Jesser, A.; dos Santos Vieira, I.; Schmidt, W. G.; Herres-Pawlis, S. Geometrical and optical benchmarking of copper(II) guanidine-quinoline complexes: insights from TD-DFT and many-body perturbation theory (part II). *J. Comput. Chem.* **2014**, *35*, 2146−2161.
(68) Witte, M.; Gerstmann, U.; Neuba, A.; Henkel, G.; Schmidt, W. G. Density functional theory of the Cu A -like Cu 2 S 2 diamond core in Cu 2II(NGuaS) 2 Cl 2. *J. Comput. Chem.* **2016**, *37*, 1005−1018.
(69) Grimme, S.; Antony, J.; Ehrlich, S.; Krieg, H. A consistent and accurate ab initio parametrization of density functional dispersion correction (DFT-D) for the 94 elements H-Pu. *J. Chem. Phys.* **2010**, *132*, 154104.
(70) Grimme, S.; Ehrlich, S.; Goerigk, L. Effect of the damping function in dispersion corrected density functional theory. *J. Comput. Chem.* **2011**, *32*, 1456−1465.
(71) Becke, A. D. A new mixing of Hartree−Fock and local density-functional theories. *J. Chem. Phys.* **1993**, *98*, 1372.
(72) Becke, A. D. Density-functional thermochemistry.III. The role of exact exchange. *J. Chem. Phys.* **1993**, *98*, 5648.
(73) Lee, C.; Yang, W.; Parr, R. G. Development of the Colle-Salvetti correlation-energy formula into a functional of the electron density. *Phys. Rev. B: Condens. Matter Mater. Phys.* **1988**, *37*, 785−789.
(74) Vosko, S. H.; Wilk, L.; Nusair, M. Accurate spin-dependent electron liquid correlation energies for local spin density calculations: a critical analysis. *Can. J. Phys.* **1980**, *58*, 1200−1211.
(75) Becke, A. D. Density-functional exchange-energy approximation with correct asymptotic behavior. *Phys. Rev. A: At., Mol., Opt. Phys.* **1988**, *38*, 3098−3100.
(76) Perdew, J. P. Density-functional approximation for the correlation energy of the inhomogeneous electron gas. *Phys. Rev. B: Condens. Matter Mater. Phys.* **1986**, *33*, 8822−8824.
(77) Perdew, J. P.; Burke, K.; Ernzerhof, M. Generalized Gradient Approximation Made Simple. *Phys. Rev. Lett.* **1996**, *77*, 3865−3868.
(78) Neese, F.; Wennmohs, F.; Hansen, A.; Becker, U. Efficient, approximate and parallel Hartree-Fock and hybrid DFT calculations. A 'chain-of-spheres' algorithm for the Hartree-Fock exchange. *Chem. Phys.* **2009**, *356*, 98−109.
(79) Neese, F. An improvement of the resolution of the identity approximation for the formation of the Coulomb matrix. *J. Comput. Chem.* **2003**, *24*, 1740−1747.
(80) Delgado-Jaime, M. U.; DeBeer, S. Expedited analysis of DFT outputs: Introducing moanalyzer. *J. Comput. Chem.* **2012**, *33*, 2180−2185.
(81) Bunău, O.; Joly, Y. Self-consistent aspects of x-ray absorption calculations. *J. Phys.: Condens. Matter* **2009**, *21*, 345501.
(82) Pasquali, M.; Floriani, C.; Venturi, G.; Gaetani-Manfredotti, A.; Chiesi-Villa, A. Copper(I)-carbon monoxide chemistry: genesis and chemical and structural properties of copper(I) terminal and bridging carbonyls. *J. Am. Chem. Soc.* **1982**, *104*, 4092−4099.
(83) York, J. T.; Brown, E. C.; Tolman, W. B. Characterization of a Complex Comprising a {Cu2(S2)2}2+ Core: Bis(μ-S22−)dicopper-(III) or Bis(μ-S2.−)dicopper(II)? *Angew. Chem., Int. Ed.* **2005**, *44*, 7745−7748.
(84) Yang, L.; Powell, D. R.; Houser, R. P. Structural variation in copper(i) complexes with pyridylmethylamide ligands: structural analysis with a new four-coordinate geometry index, τ_4. *Dalton Trans.* **2007**, 955−964.
(85) Johann, H. H. Die Erzeugung lichtstarker Röntgenspektren mit Hilfe von Konkavkristallen. *Eur. Phys. J. A* **1931**, *69*, 185−206.
(86) Hämäläinen, K.; Siddons, D. P.; Hastings, J. B.; Berman, L. E. Elimination of the inner-shell lifetime broadening in x-ray-absorption spectroscopy. *Phys. Rev. Lett.* **1991**, *67*, 2850−2853.
(87) Carra, P.; Fabrizio, M.; Thole, B. T. High Resolution X-Ray Resonant Raman Scattering. *Phys. Rev. Lett.* **1995**, *74*, 3700−3703.
(88) Loeffen, P. W.; Pettifer, R. F.; Müllender, S.; van Veenendaal, M. A.; Röhler, J.; Sivia, D. S. Deconvolution of lifetime broadening at rare-earth LIII edges compared to resonant inelastic x-ray scattering measurements. *Phys. Rev. B: Condens. Matter Mater. Phys.* **1996**, *54*, 14877−14880.
(89) Tanaka, S.; Okada, K.; Kotani, A. Resonant X-Ray Emission Spectroscopy in Dy Compounds. *J. Phys. Soc. Jpn.* **1994**, *63*, 2780−2787.
(90) Kau, L. S.; Spira-Solomon, D. J.; Penner-Hahn, J. E.; Hodgson, K. O.; Solomon, E. I. X-ray absorption edge determination of the oxidation state and coordination number of copper. Application to the type 3 site in Rhus vernicifera laccase and its reaction with oxygen. *J. Am. Chem. Soc.* **1987**, *109*, 6433−6442.
(91) Sarangi, R.; Yang, L.; Winikoff, S. G.; Gagliardi, L.; Cramer, C. J.; Tolman, W. B.; Solomon, E. I. X-ray absorption spectroscopic and

DOI: 10.1021/acs.inorgchem.6b01704
Inorg. Chem. 2016, 55, 11694−11706

computational investigation of a possible S···S interaction in the [Cu3S2]3+ core. *J. Am. Chem. Soc.* **2011**, *133*, 17180−17191.
(92) Tomson, N. C.; Williams, K. D.; Dai, X.; Sproules, S.; DeBeer, S.; Warren, T. H.; Wieghardt, K. Re-evaluating the Cu K pre-edge XAS transition in complexes with covalent metal−ligand interactions. *Chem. Sci.* **2015**, *6*, 2474−2487.
(93) Walroth, R. C.; Uebler, J. W. H.; Lancaster, K. M. Probing Cu I in homogeneous catalysis using high-energy-resolution fluorescence-detected X-ray absorption spectroscopy. *Chem. Commun.* **2015**, *51*, 9864−9867.
(94) Ray, K.; Petrenko, T.; Wieghardt, K.; Neese, F. Joint spectroscopic and theoretical investigations of transition metal complexes involving non-innocent ligands. *Dalton transactions (Cambridge, England: 2003)* **2007**, 1552−1566.
(95) Ressler, T.; Wong, J.; Roos, J.; Smith, I. L. Quantitative speciation of mn-bearing particulates emitted from autos burning (methylcyclopentadienyl) manganese tricarbonyl-added gasolines using XANES spectroscopy. *Environ. Sci. Technol.* **2000**, *34*, 950−958.
(96) Datta, S.; Rule, A. M.; Mihalic, J. N.; Chillrud, S. N.; Bostick, B. C.; Ramos-Bonilla, J. P.; Han, I.; Polyak, L. M.; Geyh, A. S.; Breysse, P. N. Use of X-ray Absorption Spectroscopy To Speciate Manganese in Airborne Particulate Matter from Five Counties Across the United States. *Environ. Sci. Technol.* **2012**, *46*, 3101−3109.
(97) Bressler, C.; Chergui, M. Ultrafast X-ray Absorption Spectroscopy. *Chem. Rev.* **2004**, *104*, 1781−1812.
(98) Canton, S. E.; Kjær, K. S.; Vankó, G.; van Driel, T. B.; Adachi, S.-i.; Bordage, A.; Bressler, C.; Chabera, P.; Christensen, M.; Dohn, A. O.; Galler, A.; Gawelda, W.; Gosztola, D.; Haldrup, K.; Harlang, T.; Liu, Y.; Møller, K. B.; Németh, Z.; Nozawa, S.; Pápai, M.; Sato, T.; Sato, T.; Suarez-Alcantara, K.; Togashi, T.; Tono, K.; Uhlig, J.; Vithanage, D. A.; Wärnmark, K.; Yabashi, M.; Zhang, J.; Sundström, V.; Nielsen, M. M. Visualizing the non-equilibrium dynamics of photoinduced intramolecular electron transfer with femtosecond X-ray pulses. *Nat. Commun.* **2015**, *6*, 6359.
(99) Milne, C. J.; Pham, V.-T.; Gawelda, W.; van der Veen, R. M.; Nahhas, A. E.; Johnson, S. L.; Beaud, P.; Ingold, G.; Lima, F.; Vithanage, D. A.; Benfatto, M.; Grolimund, D.; Borca, C.; Kaiser, M.; Hauser, A.; Abela, R.; Bressler, C.; Chergui, M. Time-resolved x-ray absorption spectroscopy: Watching atoms dance. *J. Phys. Conf. Ser.* **2009**, *190*, 012052.
(100) Penfold, T. J.; Karlsson, S.; Capano, G.; Lima, F. A.; Rittmann, J.; Reinhard, M.; Rittmann-Frank, M. H.; Braem, O.; Baranoff, E.; Abela, R.; Tavernelli, I.; Rothlisberger, U.; Milne, C. J.; Chergui, M. Solvent-Induced Luminescence Quenching: Static and Time-Resolved X-Ray Absorption Spectroscopy of a Copper(I) Phenanthroline Complex. *J. Phys. Chem. A* **2013**, *117*, 4591−4601.

DOI: 10.1021/acs.inorgchem.6b01704
Inorg. Chem. 2016, 55, 11694−11706